THE JOURNAL OF PHYSICAL CHEMISTRY A

Article

pubs.acs.org/JPCA

Interaction of CO_2 with Atomic Manganese in the Presence of an Excess Negative Charge Probed by Infrared Spectroscopy of $[Mn(CO_2)_n]^-$ Clusters

Michael C. Thompson, Jacob Ramsay, and J. Mathias Weber*

JILA and Department of Chemistry and Biochemistry, University of Colorado, Boulder, Colorado 80309-0440, United States

Supporting Information

ABSTRACT: We report infrared photodissociation spectra of manganese−CO_2 cluster anions, $[Mn(CO_2)_n]^-$ (n = 2−10) to probe structural motifs characterizing the interaction between Mn and CO_2 in the presence of an excess electron. We interpret the experimental spectra through comparison with infrared spectra predicted from density functional theory calculations. The cluster anions consist of core ions combining a Mn atom with a variety of ligands, solvated by additional CO_2 molecules. Structural motifs of ligands evolve with increasing cluster size from simple monodentate and bidentate CO_2 ligands to oxalate ligands and combinations of these structural themes.

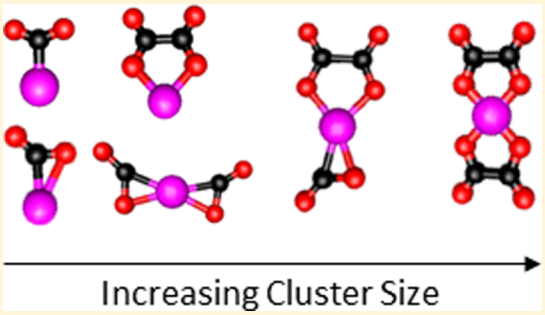

INTRODUCTION

The interaction of CO_2 with metal atoms is an important aspect in the catalytic conversion of CO_2 by metal surfaces, metal complexes, and metal-containing active centers in proteins. In this context, manganese complexes are of interest for CO_2 reduction and for adsorption in metal−organic frameworks.[1−4] In the case of conversion of CO_2 to CO at metal electrode catalysts, the proposed rate-limiting step is the addition of a single electron to CO_2.[5,6] While manganese is not commonly used in metal electrodes for the purpose of CO_2 reduction, metal organic Mn complexes have been shown to be CO_2 reduction catalysts.[3,7] In such complexes, the access of CO_2 to the metal atoms is restricted by the rest of the chemical environment, e.g., ligands in metal organic complexes. It is of fundamental interest to study the interaction of CO_2 with metal atoms, without limiting access of CO_2 molecules to the metal atom, e.g., by the presence other ligands. This can be achieved by investigating metal−CO_2 interactions in gas phase clusters.

Mass spectrometry, ion−molecule collision studies, and infrared spectroscopy of mass selected cluster ions have been particularly powerful tools to obtain information on metal−CO_2 interactions.[8−14] Work on transition metal−CO_2 cluster ions has shown that in most cationic metal−CO_2 clusters the metal−CO_2 interaction is governed by electrostatic forces,[9,15−19] with few exceptions[20] unless the collision energies are sufficiently high to allow insertion of metal atoms into CO bonds.[21] In contrast, anionic metal−CO_2 clusters show complex and intriguing chemistry with the formation of a diverse set of CO_2-based ligands.[8,22−27] In this article, we present experimental and computational work to determine the nature of the interaction between CO_2 and manganese atoms in the presence of an excess electron. Using IR photodissociation spectroscopy, we investigate possible binding motifs of CO_2 to manganese along with the influence of solvation on the charge distribution of these manganese−CO_2 complexes.

METHODS

Experimental Section. Our experimental setup has been described in detail previously.[28] Briefly, Mn vapor was generated by irradiating a rotating Mn disk target with the third harmonic of a pulsed Nd:YAG laser (355 nm; 40 mJ/pulse). The vapor was entrained into a pulsed supersonic expansion of CO_2 (stagnation pressure 550 kPa) generated by an Even−Lavie valve. This resulted in the formation of $[Mn(CO_2)_n]^-$ clusters along with $(CO_2)_n^-$ clusters and other species (see Supporting Information). The anionic products of the ion source were injected into a Wiley−McLaren type mass spectrometer. The ions of interest were mass-selected using a pulsed mass gate and irradiated in a multipass cell by the output of a tunable OPO/OPA system in the range of 1000−2150 cm^{-1} and 2200−2400 cm^{-1} with a bandwidth of ca. 2 cm^{-1} and a pulse duration of 7 ns. The formation of fragment ions due to the loss of a single CO_2 molecule was monitored using a reflectron as a secondary mass analyzer, and the fragments were detected using a microchannel plate detector. Action spectra were generated by monitoring the formation of fragment ions as a function of photon energy and corrected for photon fluence. Multiple spectra were recorded on several days and averaged in order to increase the signal-to-noise ratio and ensure reproducibility. The experiment was operated at a repetition rate of 20 Hz.

Received: July 12, 2017
Revised: September 11, 2017
Published: September 19, 2017

DOI: 10.1021/acs.jpca.7b06870
J. Phys. Chem. A 2017, 121, 7534−7542

Computational. Calculations were performed using the TURBOMOLE V. 5.9.5 suite of programs in order to explore structural motifs of $[Mn(CO_2)_n]^-$ clusters.[29] The B3LYP functional[30,31] with dispersion correction[32] was employed for all calculations, and def2-TZVPP[33] basis sets were used for all atoms. Vibrational frequencies were calculated with the AOFORCE[34] program, and were scaled by 0.9752 for all modes, except the asymmetric stretching motion of metalloformate type species. For the latter, a scaling factor of 0.9380 was used based on calculations by Boese et al. for the corresponding vibrational motion in $[AuCO_2]^-$.[35] Simulated spectra were generated by representing the scaled calculated transitions with Gaussians (12 cm^{-1} full width at half-maximum). Partial charges were obtained using natural population analysis.[36]

RESULTS AND DISCUSSION

Overview. Experimental spectra for $[Mn(CO_2)_n]^-$ (n = 2−10) are shown in Figure 1 and show a pronounced change with

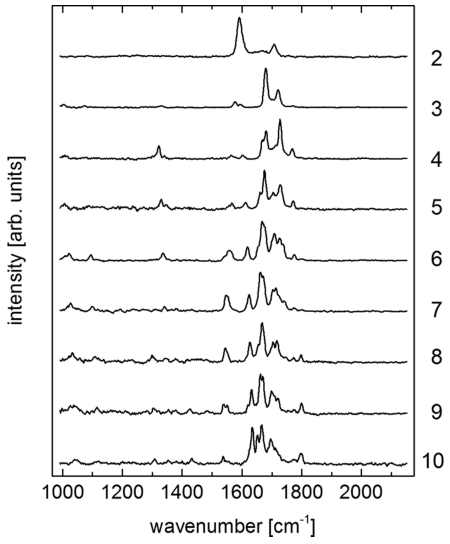

Figure 1. Photodissociation spectra of $[Mn(CO_2)_n]^-$ cluster ions (n = 2−10, see numbers on right), obtained by monitoring the loss of one CO_2 unit. Each spectrum is scaled to its strongest feature.

cluster size, particularly between n = 2 and 4. The infrared transitions are due to CO stretching vibrations of the clusters and reflect the interaction of the individual CO_2 moieties with the metal as well as the charge distribution in the complex. Individual CO_2 molecules can act either as a solvent of the core ion or as part of the core ion itself. Previous work on anionic clusters containing CO_2 showed[8,22−27] that solvent CO_2 molecules are only weakly perturbed, having antisymmetric stretching frequencies slightly below the neutral gas phase value[37] of 2349 cm^{-1} due to the vicinity of the core anion. Transitions in the region 2320−2350 cm^{-1} are evidence of at least one CO_2 molecule acting as a solvent species.[38] We will address the spectra in this region in more detail in our discussion of the behavior of the larger clusters.

In contrast to CO_2 solvent molecules, CO_2 ligands bonded directly to the metal have substantial partial negative charge, as seen in studies of CO_2 with other d-block metals.[23−25,27] From the point of view of a CO_2 functional group, this excess charge is accommodated in the $6a_1$ antibonding orbital,[39] which weakens the CO bonds compared to neutral CO_2 and results in a strong red shift of the CO stretching frequencies compared to neutral CO_2. Transitions in the region 1000−2150 cm^{-1} are indicative of one or more CO_2 ligands being part of the core anion of the cluster, and the frequency positions depend on the character of the interaction between the CO_2 ligands and the metal center.[8,22−26] The signatures from 1600 to 1750 cm^{-1} in the spectra of $[Mn(CO_2)_n]^-$ clusters become increasingly complex as the cluster size increases, particularly in the size region from n = 2 to n = 4. This increase in complexity can be due to two effects or combinations thereof: (i) the core ion can be very polarizable, and different solvent conformations can substantially change the charge distribution of the core ion, resulting in shifts of corresponding infrared signatures;[8,22,23,25,26] (ii) multiple conformers of the core ion itself can develop with increasing cluster size.[23,27]

It is important to note that we obtain the photodissociation spectra of $[Mn(CO_2)_n]^-$ clusters by monitoring the loss of CO_2 molecules upon photon absorption. Therefore, the binding energy of these CO_2 molecules limits the spectral range in this experiment. A single CO_2 molecule solvating one of the possible core ions in this work has a calculated binding energy of ca. 1500 cm^{-1}, and this binding energy diminishes by ca. 100 cm^{-1} with each increasing solvent molecule. Due to the internal energy in the cluster prior to photon absorption, photon energies lower than this threshold can still result in dissociation. However, the photodissociation efficiency at photon energies below the threshold for loss of a CO_2 molecule is no longer unity, and features at lower energies are suppressed in the experimental spectra, particularly for the smaller clusters. The binding energy of a CO_2 ligand that is part of the core ion is of the order of 10^4 cm^{-1}. This is much larger than the photon energies accessible in this experiment, and as a result, we cannot probe the structure of an unsolvated complex anion.

Manganese has the electron configuration $4s^23d^5$. Together with the excess electron in the complex, this can result in singlet, triplet, or quintet spin states. All calculated structures were computed in all three spin states in order to determine their relative energies and potential differences in geometry and vibrational spectra. In all cases, the quintet structures were lowest in energy, followed by the triplet structures, with the singlet structures being highest in energy, as expected by simple electron−electron repulsion arguments. At the same time, there are no significant geometry differences between different spin states of the same structural family, suggesting that the energy differences are solely due to the electron configuration, with little to no geometry changes. As we will discuss in detail for cluster size n = 3, our experimental spectra provide some evidence that the spectroscopic features we observe are due to quintet states. Even if the calculated spectra for some core ions are not sensitive to spin state, we assume that all core ions are in quintet states. All structures presented in the remainder of this article are therefore of quintet multiplicity unless stated otherwise.

$[Mn(CO_2)_2]^-$. As mentioned above, the binding energy of a CO_2 ligand bound to a metal atom is too high to photodissociate an unsolvated core ion species that contains two strongly bound CO_2 ligands. Therefore, the experimental spectrum of $[Mn(CO_2)_2]^-$ reflects the vibrational signatures of solvated $[MnCO_2]^-$. The spectrum for $[Mn(CO_2)_2]^-$ has signatures in both the core and the solvent regions (see later discussion), in line with this expectation.

There are two strong transitions in the experimental spectrum of $[Mn(CO_2)_2]^-$, one at 1592 cm^{-1} and another at 1710 cm^{-1}, with a broad, unresolved feature in between. A

DOI: 10.1021/acs.jpca.7b06870
J. Phys. Chem. A 2017, 121, 7534−7542

search for local minimum energy structures of a $[MnCO_2]^-$ core ion revealed three structures that can recover features in the experimental spectrum (see Figure 2 for notation).

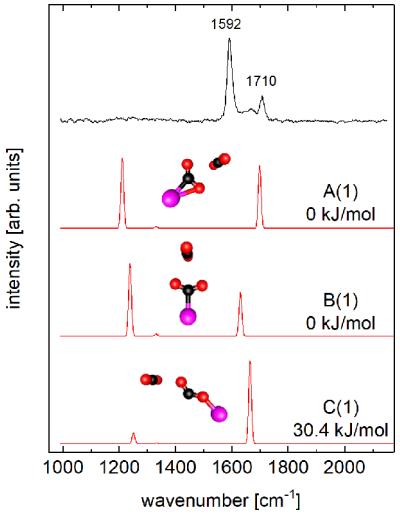

Figure 2. Comparison of the calculated spectra for different calculated isomers of $[Mn(CO_2)_2]^-$ (lower traces, all in quintet states) to the experimental spectrum for $[Mn(CO_2)_2]^-$ (top trace). Capital letters denote the core ion structure, and numbers in parentheses denote the number of solvent species. Energies are given relative to the isoenergetic isomers A(1) and B(1). No other minimum energy structures containing a solvent CO_2 molecule were found at this cluster size regarding core ions or solvent isomers. Mn atoms are shown in purple, C atoms in black, and O atoms in red.

Structure B(1) can be characterized as a metalloformate (η^1 type ligand), where the C atom forms a covalent bond with the Mn atom, and the two CO groups point away from the metal. The A(1) family has a bidentate structure (η^2 type ligand), where the CO_2 ligand forms both C−Mn and O−Mn bonds. We note that A(1) and B(1) are calculated to lie within 1 meV (0.1 kJ/mol) and can be seen as isoenergetic.

As mentioned earlier, we assume that all complexes have quintet configurations, but we note that we cannot exclude the other spin states purely on spectroscopic grounds for $[Mn(CO_2)_2]^-$, since the spectra look very similar for all spin configurations (see Supporting Information), and the assignment therefore rests on energy arguments as stated above. A comparison of the predicted infrared spectra of the different structures with the experimental spectrum of $[Mn(CO_2)_2]^-$ is shown in Figure 2.

We assign the features at 1592 and 1710 cm^{-1} to the antisymmetric stretching modes of B(1) and A(1), respectively. The feature at 1592 cm^{-1} could in principle also be due to C(1), where the CO_2 unit is bound to the Mn via the oxygen atom, and the ligand is effectively a CO_2 anion. However, we will show in the following that this is unlikely.

In order to investigate the origin of the broad feature between the two intense peaks, we calculated a potential energy curve by varying the C−Mn−O bond angle, θ, while allowing all other coordinates to relax. This Born−Oppenheimer potential energy curve, $U_{BO}(\theta)$, connects the different quintet structures, and allows inspection of the barriers toward interconversion between them (see Figure 3). Surprisingly, $U_{BO}(\theta)$ is very flat, with almost no change in energy over a range of 80°, suggesting that the CO_2 rocking mode carries

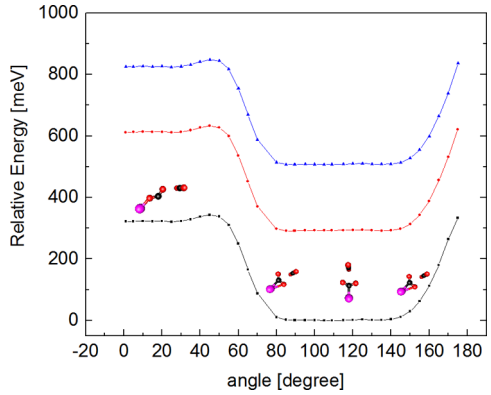

Figure 3. Potential energy surfaces along the Mn−C−O bond angle for $[Mn(CO_2)_2]^-$. The Born−Oppenheimer curve , vibrationally adiabatic ground state, and vibrationally excited surface belonging to the antisymmetric CO stretching mode are shown in black, red, and blue, respectively (see text for details). Note that the vibrational frequencies were not scaled for the construction of these potential energy surfaces.

large amplitudes, even at very low levels of excitation. The potential energy surface also suggests a very shallow minimum (25 meV; 2.4 kJ/mol) for structure C, which likely results in quick conversion of C to A/B, i.e., leads to the formation of a Mn−C bond. Based on this observation, we assume that structure C is not reflected in the spectroscopic signatures. Constructing a vibrationally adiabatic surface along this coordinate according to the expression[40,41]

$$U_{ad,0}(\theta) = U_{BO}(\theta) + \frac{1}{2}\sum_j \hbar\omega_j \quad (1)$$

shows that the overall structure of the curve is roughly the same as of $U_{BO}(\theta)$. In this approach, the sum goes over the two CO-stretching frequencies of the ligand, since they are much faster than the CO_2 rocking frequency. The corresponding curve for the excited state with one quantum in the asymmetric CO stretching mode of the CO_2 ligand, $U_{ad,1}(\theta)$, has again the same overall structure. Unresolved sequence bands in the large amplitude CO_2 rocking vibration could explain the broad feature between the two sharper bands in the spectrum. This is reminiscent of the situation in some other systems with large amplitude motions,[41,42] but the flat potential energy surfaces, small differences in the shapes of ground and excited states, and the presumably very narrow spacing between quantum states in the flat wells likely cause the lack of resolved sequence band features. As stated above, all sharp spectral signatures in this cluster size can be described as a mixture between structures A(1) and B(1).

It is interesting to note that, for unsolvated $MnCO_2^-$, structure B(0) represents a maximum along the Mn−C−O bond angle, which is ca. 200 meV (19 kJ/mol) above the bidentate structure A(0), and A(0) is 68 meV (6.6 kJ/mol) above isomer C(0), highlighting the role of solvation.

$[Mn(CO_2)_3]^-$. The spectrum for $[Mn(CO_2)_3]^-$ has two strong peaks at 1680 and 1724 cm^{-1}, with two doublets of weaker features at 1575 cm^{-1}/1594 cm^{-1} and at 1003 cm^{-1}/1076 cm^{-1}, as well as a small peak at 1330 cm^{-1}. At this cluster size, we probe core ions with one or two strongly bound CO_2 moieties, since at least one solvent molecule needs to be present to allow photodissociation in the photon energy range of the experiment.

DOI: 10.1021/acs.jpca.7b06870
J. Phys. Chem. A 2017, 121, 7534−7542

The calculations reveal a plethora of possible structural motifs for the core ion at this cluster size (see Supporting Information), but only two core ion structures are necessary to explain the main spectroscopic features (see Figure 4). The

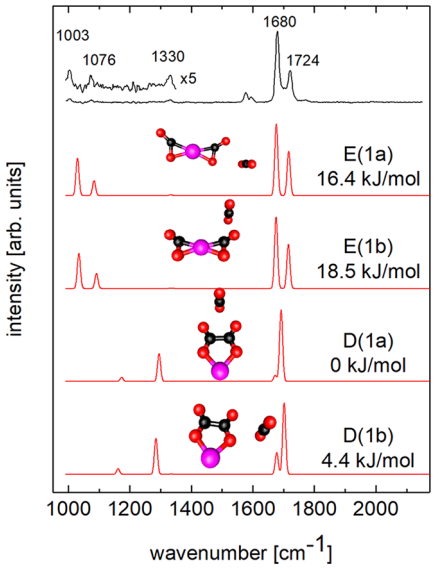

Figure 4. Comparison predicted spectra of selected calculated quintet structures (lower traces, red) to the experimental spectrum of $[Mn(CO_2)_3]^-$ (top trace, black).

lowest energy structures, D(1a,b), have two CO_2 units forming a C_2O_4 ligand and coordinating to the metal atom through two oxygen atoms (we expand the nomenclature for isomers by lowercase letters to distinguish solvent conformers). This core ion structure is reminiscent of the planar D_{2h} symmetry of several inorganic salts of the oxalate (C_2O_4) dianion.[43] In the present case, the Mn atom and the oxalate ligand in the bare complex D have partial charges of +0.72 e and −1.72 e, respectively. The configuration and charge distribution can be interpreted as an oxalate ion in a complex with a singly charged Mn cation. This structure has previously been found in other metal−CO_2 cluster anions as well.[26,27]

The structural family next higher in energy at this cluster size (E) is of the "butterfly" type, which has been identified as the main structural motif for several other first-row transition metal−CO_2 complexes.[23−25,27] Further structural families (F − H) found as core ion minimum energy structures are shown in Supporting Information, but are unlikely to significantly contribute to the spectrum at this cluster size.

A comparison of calculated frequencies of the conformers of $[Mn(CO_2)_3]^-$, discussed above, to the experimental spectrum is shown in Figure 4. The butterfly motif (E) best recovers both main spectral features at this cluster size. It also recovers the two lowest frequency features. The signatures at 1680 and 1724 cm^{-1} are due to the in-phase and out-of-phase combinations of the asymmetric CO stretching modes of the individual CO_2 ligands. The small features at 1003 and 1076 cm^{-1} are due to in-phase and out-of-phase combinations of the symmetric CO stretching modes. These features are strongly suppressed because the transition energy is lower than the binding energy of CO_2 (~1500 cm^{-1}). Based on the comparison of experimental and calculated spectra, we find that the butterfly structural motif (E) is the main contributor to the experimental spectrum. This observation is consistent with the observation in other metal−CO_2 cluster anions that high energy isomers can be kinetically trapped during ion formation.[25,27] The oxalate motif (D) probably contributes to the overall intensity of the peak at 1680 cm^{-1} and is responsible for the peak at 1330 cm^{-1}.

Interestingly, different solvent positions do not seem to significantly influence the peak positions of the butterfly isomer (E) at this cluster size. Variations in the solvent conformation around isomer D generally change the intensity ratios of the in-phase vs out-of-phase combinations of the asymmetric CO stretching vibrations, and the corresponding peak shifts are typically of the order of 10 cm^{-1}.

The transitions at 1575 and 1594 cm^{-1} may in principle be caused by solvation conformers of isomers B or H (see Supporting Information). However, their predicted features in the range of 1200−1400 cm^{-1} are not observed, and while they would almost certainly be suppressed by kinetic shift effects, the signal-to-noise ratio in the experimental spectrum would likely allow them to be observed. While we cannot unambiguously exclude that they may contribute to the absorption features around 1700 cm^{-1} at present, the origin of the peaks at 1575 and 1594 cm^{-1} remains unclear.

For core ion isomer E, the vibrational spectra of different spin states for the butterfly motif are quite different regarding both the splitting and the intensity ratio of the in-phase and out-of-phase combinations of the antisymmetric stretching modes of the two CO_2 ligands (see Figure 5). These differences confirm unambiguously that only the quintet state is populated for this isomer, in agreement with the arguments made in the overview section above.

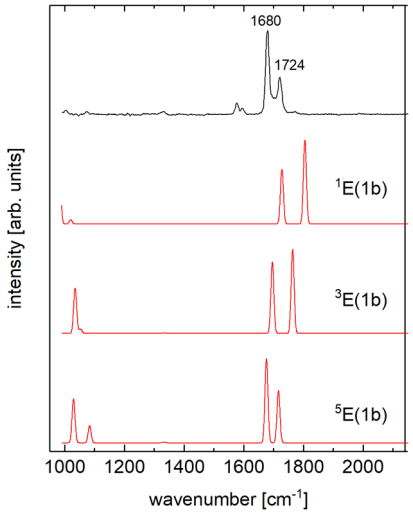

Figure 5. Calculated vibrational spectra for different spin states of structure E(1b) and the experimental spectrum of $[Mn(CO_2)_3]^-$ (top). Numbers in superscript indicate the spin state of the complex.

We note that exploratory calculations for isomer E(0) allow us to estimate a barrier height for interconversion to isomer F(0) to be at ca. 50 kJ/mol (ca. 15 kJ/mol in the reverse direction). Similarly, interconversion between isomers involving a change of connectivity (e.g., from family E to family D) is expected to have large isomerization barriers, since rather strong metal−carbon and metal−oxygen bonds have to be broken, together with a significant core ion geometry rearrangement. We therefore judge all core ion isomers we identified as relevant for $n \geq 3$ to be robust, and their predicted infrared signatures to be valid even after zero-point motion.

DOI: 10.1021/acs.jpca.7b06870
J. Phys. Chem. A 2017, 121, 7534−7542

$[Mn(CO_2)_4]^-$. At this cluster size, the spectrum becomes more complex, and prominent new spectroscopic features appear at 1321 and 1777 cm^{-1}. The lowest energy structure for this cluster size contains three CO_2 moieties (structure I, see Figure 6). It builds on the oxalate motif (D), with an additional

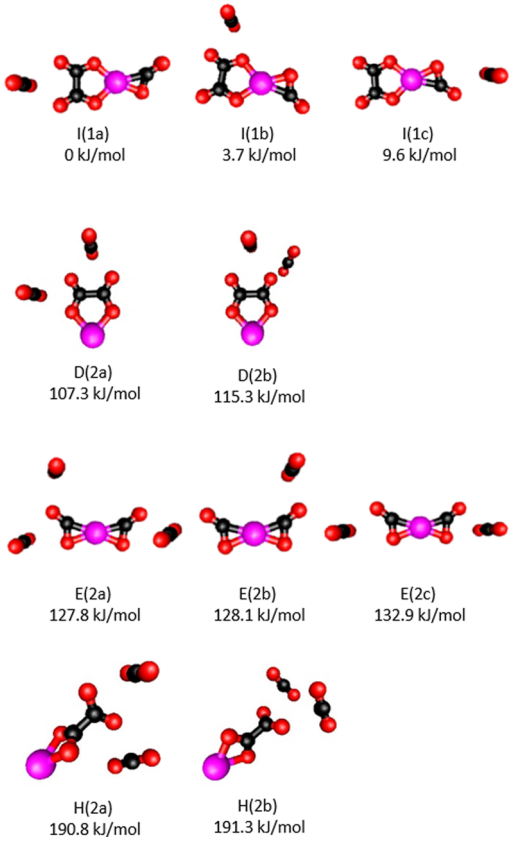

Figure 6. Calculated structures and relative energies of $[Mn(CO_2)_4]^-$ clusters. See caption of Figure 2 for nomenclature and color scheme.

bidentate CO_2 ligand opposite of the oxalate group. Other conformers are formed by adding solvent molecules to structures D(1a,b), on the oxalate side, and to the butterfly motif, E(1a,b).

The experimental spectrum for $[Mn(CO_2)_4]^-$ is presented in Figure 7 together with calculated spectra for the structures described above. The calculated spectrum with the oxalate/bidentate structural family I, particularly isomer I(1b), shows excellent agreement with the group of three peaks in the 1600–1800 cm^{-1} region, as well as the peak observed at 1321 cm^{-1}. Different solvent conformers shift the upper and lower components of the group, which may account for some of the substructure in this region. Core ion structures D and E are also compatible with some of the features in the 1600–1800 cm^{-1} range, and they may contribute to the overall absorption profile in this region.

We can assign some of the individual transitions at lower wavenumbers as follows. The peak at 1321 cm^{-1} is the in-phase combination of the symmetric CO_2 stretching modes in the oxalate group, in either structure D or I, and this motion is relatively insensitive to solvation position. The feature at 1777 cm^{-1} (the highest frequency component of the main group of peaks) is assigned to the asymmetric stretching mode of the bidentate CO_2 ligand in structure I, while the transitions between 1600 and 1750 cm^{-1} are due to in-phase and out-of-

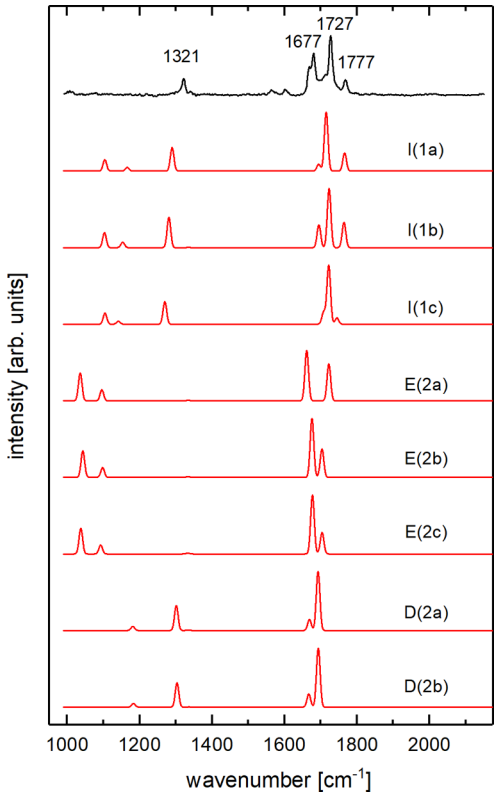

Figure 7. Comparison of the experimental spectrum of $[Mn(CO_2)_4]^-$ (upper trace) with calculated spectra of several structural isomers (lower traces). See Figure 6 for structures.

phase combinations of asymmetric CO stretching motions in the C_2O_4 moiety. Similar to the behavior of core ion structure D, peak positions and relative intensities for structure I are weakly influenced by the position of the CO_2 solvent.

The butterfly motif (E) very likely also contributes to the spectrum, and we assign the weak signatures at 1003 and 1076 cm^{-1} to this core ion, similar to the low energy peaks observed for n = 3. The solvent conformations at this cluster size are calculated to have a stronger influence on the peak positions for this core ion. In particular, asymmetric solvation around one of the bidentate CO_2 ligands results in an increased localization of the mode onto single CO_2 ligands. The "in-phase" mode becomes localized on the unsolvated ligand, while the "out-of-phase" mode mainly involves the CO oscillators on the solvated ligand. This localization is concomitant with an increase of the splitting between the "in-phase" and "out-of-phase" modes, as the partial charges on the two ligands differ due to the asymmetry in the solvation. Structures based on core ion E are much higher in energy than the oxalate/bidentate structures, but we assume that core ion E is kinetically trapped, since isomerization from this core ion into others would require Mn–C bonds to break. Judging from our calculations on $MnCO_2^-$ (see Figure 4), this is associated with a barrier of at least ca. 350 meV (34 kJ/mol).

For structure D, our calculations suggest that solvation of this core ion directly at the metal atom during cluster formation results in the formation of structure I. Isomers D(2a) and D(2b) are roughly 1 eV higher in energy than structures I(1a–c), since the Mn–O and Mn–C bonds to the bidentate ligand stabilize core ion I relative to core ion D. This implies that as the number of solvents increases, it becomes more and more

DOI: 10.1021/acs.jpca.7b06870
J. Phys. Chem. A 2017, 121, 7534–7542

likely that core ion I will be formed, while core ion D will be less populated as solvation sites become occupied around the oxalate motif. We assume that structure D isomerizes to structure I as the cluster size increases.

Similar to $[Mn(CO_2)_3]^-$, the two weak signatures just below the main group of peaks (1562 and 1604 cm^{-1}) are compatible with contributions from core ions B or H (see Supporting Information). However, as mentioned above, these core ions have additional predicted signatures at lower wavenumbers, which should be observable with similar intensities as the peak found at 1321 cm^{-1}. The narrow width of this peak, however, suggests that it is not a composite feature with contributions from several core ion isomers. We will therefore refrain from assigning the two features at 1562 and 1604 cm^{-1}.

Larger Clusters. There are only small changes upon further increase of cluster size. In particular, the relative intensities of features below 1300 cm^{-1} seems to increase. This can be rationalized with the decreasing binding energy of CO_2 solvent molecules at increasing cluster size. Note that this diminishing of kinetic shift effects is more pronounced for smaller core ion structures, since they will have more solvent molecules at the same cluster size.

Interestingly, the observation of new core ion isomers also becomes possible. In particular, a core ion with two oxalate ligands (J) is now the lowest energy calculated isomer. This structure differs from structure D in that the individual oxalate ligands and metal atom have a charge of −1.289 e and +1.60 e, respectively. While the individual oxalate ligands have a lower amount of charge compared to the single oxalate complexes (∼−1.5 e), the combined presence of both oxalate ligands results in a large amount of positive charge on the Mn atom. Two additional new core ion isomers based on C_2O_4 ligands were also found, a core ion with one D_{2d} and one D_{2h} oxalate ligand (K) and a core ion with two D_{2d} ligands (L) (see Supporting Information). Both of these structures are very high in energy, and calculated vibrational frequencies are not consistent with the experimental spectrum. Calculated core ion structures and their relative energies of selected core ion geometries are provided in Figure 8.

The experimental spectrum of $[Mn(CO_2)_5]^-$ is shown in Figure 9 along with the calculated spectra of several isomers. As with the smaller cluster sizes, most features of the experimental spectrum are recovered with various solvent configurations around core ion geometries that have already been discussed. In particular, we expect core ion structures E and I to play dominant roles in the spectra of the larger clusters, since a conversion of structures formed with bidentate ligands to oxalate ligands will involve a significant isomerization barrier (see discussion above). Core isomer J may contribute to the intense peak at 1728 cm^{-1}. Since it has only one solvent molecule, the predicted lower energy feature may be too strongly suppressed by CO_2 binding energy effects to appear in the spectrum.

The tendency of the larger clusters to form oxalate ligands is interesting, since it suggests a strong affinity to CO_2, with a preference toward highly charged ligands. We note that in complexes that contain two oxalate ligands (either in the planar D_{2h} configuration or the D_{2d} configuration) the metal atom has a charge of at least +1.5 e. By incorporating larger CO_2 moieties into the complex, the manganese atom is able to donate more electron density to the ligands, resulting in further oxidation of the metal center, reflecting its tendency to realize higher oxidation states.

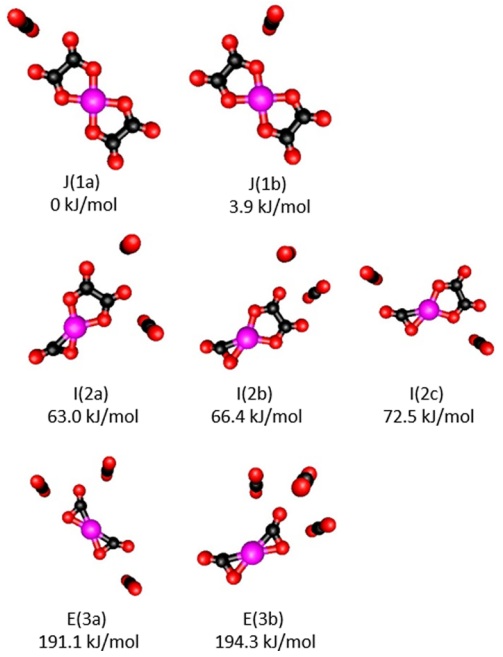

Figure 8. Selected structures and relative energies for $[Mn(CO_2)_5]^-$, ordered from top to bottom along increasing numbers of solvent molecules.

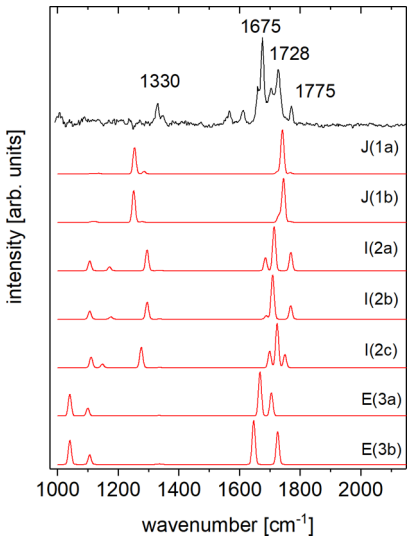

Figure 9. Comparison of the experimental spectrum of $[Mn(CO_2)_5]^-$ (upper trace) with calculated spectra of several structural isomers (lower traces). See Figure 8 for structures.

The spectra of the larger clusters show some more complexity in the region of the dominant signatures (1600–1800 cm^{-1}), as some of the peaks in this region split and develop more shoulders with increasing cluster size. This behavior can be traced to the solvent conformation dependence of some of the main core ion structures. The spectroscopic patterns of the oxalate and bidentate containing core ions discussed above (e.g., structures E and I) exhibit a clear dependence on solvent conformation. This solvation dependence is very likely at the heart of the splitting and shifts observed for the larger clusters, reminiscent of the behavior of $[Cu(CO_2)_n]^-$ cluster ions.[23] Given the large spectral congestion

DOI: 10.1021/acs.jpca.7b06870
J. Phys. Chem. A 2017, 121, 7534−7542

of the dominant spectral region, we refrain from assigning individual signatures to specific solvent conformers.

The structures found in $[Mn(CO_2)_n]^-$ clusters based on bidentate and oxalate ligands are consistent with the structures found in clusters containing other first row transition metals (Fe, Co, Ni, and Cu).[23−25,27] It is clear that the first row transition metals share common binding motifs to CO_2, specifically a preference for the η^2 bonding scheme. This is different from clusters of CO_2 with coinage metals (Ag and Au),[8,22] where the dominant binding motif is a metalloformate structure.

The region that is characteristic for solvent features, i.e., around 2350 cm^{-1}, is interesting in $[Mn(CO_2)_n]^-$ clusters. The antisymmetric stretching mode of free CO_2 is at 2349 cm^{-1}, and the corresponding signatures of solvent CO_2 molecules are typically found slightly to the red of this mark, since solvation of anions by CO_2 involves a small amount of charge transfer onto the solvent.[44] With an increasing number of solvent molecules, the charge transfer per solvent molecule typically diminishes, and the antisymmetric stretching vibrational modes of the solvent molecules shift toward increasing wavenumbers as a result. This behavior has been observed in all other metal−CO_2 cluster anions so far,[8,22−27] although some cluster systems exhibit some substructure in the solvent region that is likely due to inequivalent solvent positions. One of the components observed in the solvent region in $[Mn(CO_2)_n]^-$ clusters follows this expected trend, staying to the red of the antisymmetric stretching mode of free CO_2. Different from other metal−CO_2 cluster anions, the larger $[Mn(CO_2)_n]^-$ clusters develop an additional signature that is clearly blue-shifted compared to the frequency of neutral CO_2 (see Figure 10), and can reach peak

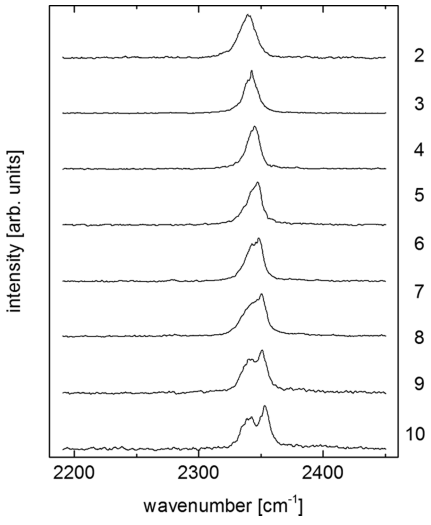

Figure 10. Infrared spectra of $[Mn(CO_2)_n]^-$ in the region characteristic for solvent features. The cluster size is indicated by the numbers on the right.

positions as high as 2354 cm^{-1}. This blue shift relative to free CO_2 is reminiscent of metal−CO_2 cluster cations,[16,45,46] where CO_2 molecules bind to a cation via M−O interactions, keeping the CO_2 molecules linear. Metal organic complexes can also accommodate CO_2 as a ligand in such a configuration. In exploratory calculations on $[Mn(CO_2)_9]^-$ with core ion structure J, we found a minimum energy structure with four solvent molecules around the equatorial oxalate ligands, and one solvent above the plane of the core ion (see Supporting Information). The calculated antisymmetric stretching mode of this additional solvent molecule is at 2355 cm^{-1}. The presence of a solvent molecule close to the metal atom could therefore account for the blue-shifted signature in the spectra of the larger clusters. We note that the solvent above the plane of the core ion is not along the axis of the complex and cannot be classified as being in an axial position.

Calculated Size Evolution of Core Ion Structures. Since the present experiment is only sensitive to clusters with at least one weakly bound CO_2 molecule, it is of interest to compare the calculated lowest energy cluster structures for each cluster size with those experimentally observed (summarized in Table 1).

Table 1. Size Evolution of Calculated Unsolvated and Solvated Lowest Energy Structures, and Comparison with Experimental Observations for n = 1−5

n	calcd lowest energy structure	lowest solvated structure at n + 1	experimentally obsd at n + 1?
1	C(0) (O-monodentate)	A(1), B(1)	no
2	D(0) (oxalato)	D(1)	yes
3	I(0) (oxalato/bidentate)	I(1)	yes
4	J(0) (bioxalato)	J(1)	yes
5	J(1) (bioxalato)		

As mentioned earlier, the global minimum structure for unsolvated $MnCO_2^-$ (i.e., n = 1) is structure C(0), which is transformed upon solvation into the least stable structure for n = 2. As a consequence, the lone solvent molecule at n = 2 drastically affects the core ion structure, and the lowest energy structure for n = 1 is not even observed at n = 2 in the experiment. In contrast, for bare core ions at n = 2, the lowest energy structure is D(0), the Mn−oxalato complex, which is calculated to be the lowest energy solvated core ion and is experimentally observed at n = 3. Similarly, for the larger clusters, the calculated minimum energy structure at size n corresponds to the lowest energy solvated core ion structure at size (n + 1), and they are observed experimentally as well. As a result of this comparison, we conclude that while a CO_2 molecule solvating $MnCO_2^-$ will change the core ion structure, the core ions in larger clusters are robust with respect to solvation.

CONCLUSIONS

The structures of the dominant core ions in $[Mn(CO_2)_n]^-$ clusters depend on the number of CO_2 molecules in the cluster anion. Structural families evolve from a single CO_2 moiety bound as a formate or bidentate ligand through butterfly type and oxalate to combinations of these two as main structural themes. Our calculations suggest that there is a tendency toward incorporation of an increasing number of CO_2 moieties into the core ion with increasing cluster size, up to four CO_2 molecules in the form of two C_2O_4 ligands. The structural behavior is similar to that of other first-row transition metals, particularly to that found in Fe−CO_2 cluster anions.[27] The later transition metals (Co, Ni, Cu) tend to bind CO_2 predominantly by forming bidentate interactions involving metal−carbon and metal−oxygen bonds.[23−25] The later coinage metals (Ag, Au) are distinctly different, forming mainly metalloformate complexes with single CO_2 ligands.[8,22] Spectroscopic evidence points to the preferential population quintet spin states.

DOI: 10.1021/acs.jpca.7b06870
J. Phys. Chem. A 2017, 121, 7534−7542

Overall, manganese−CO_2 cluster anions can be characterized as metal organic complexes with bidentate and oxalate ligands in mostly planar configurations, with an intriguing richness of available structures.

■ ASSOCIATED CONTENT

Supporting Information

The Supporting Information is available free of charge on the ACS Publications website at DOI: 10.1021/acs.jpca.7b06870.

Mass spectrum, calculated spectra and relative energies, and coordinates and vibrational frequencies (PDF)

■ AUTHOR INFORMATION

Corresponding Author

*E-mail: weberjm@jila.colorado.edu. Phone: ++1-303-492-7841.

ORCID

J. Mathias Weber: 0000-0002-5493-5886

Notes

The authors declare no competing financial interest.

■ ACKNOWLEDGMENTS

We gratefully acknowledge funding from the National Science Foundation (NSF) through the NSF AMO Physics Frontier Center at JILA (PHY-1125844 and PHY-1734006). We also acknowledge graduate student support from the U.S. Department of Education through a GAANN Fellowship for M.C.T.

■ REFERENCES

(1) Jiang, J.; Wang, Q.; Zhang, M.; Bai, J. A Distorted $[Mn_2(COO)_4N_2]$ Cluster Based Metal−Organic Framework with (3,3,6) Topology and Selective Adsorption of CO_2. *Cryst. Growth Des.* **2017**, *17* (4), 2223−2227.

(2) Fei, H.; Sampson, M. D.; Lee, Y.; Kubiak, C. P.; Cohen, S. M. Photocatalytic CO_2 Reduction to Formate Using a Mn(I) Molecular Catalyst in a Robust Metal−Organic Framework. *Inorg. Chem.* **2015**, *54* (14), 6821−6828.

(3) Sampson, M. D.; Nguyen, A. D.; Grice, K. A.; Moore, C. E.; Rheingold, A. L.; Kubiak, C. P. Manganese Catalysts with Bulky Bipyridine Ligands for the Electrocatalytic Reduction of Carbon Dioxide: Eliminating Dimerization and Altering Catalysis. *J. Am. Chem. Soc.* **2014**, *136* (14), 5460−5471.

(4) Rosser, T. E.; Windle, C. D.; Reisner, E. Electrocatalytic and Solar-Driven CO_2 Reduction to CO with a Molecular Manganese Catalyst Immobilized on Mesoporous TiO_2. *Angew. Chem., Int. Ed.* **2016**, *55* (26), 7388−7392.

(5) Bockris, J. O'M.; Wass, J. C. The Photoelectrocatalytic Reduction of Carbon Dioxide. *J. Electrochem. Soc.* **1989**, *136* (9), 2521−2528.

(6) Chandrasekaran, K.; Bockris, L. O. M. In-Situ Spectroscopic Investigation of Adsorbed Intermediate Radicals in Electrochemical Reactions: CO_2^- on Platinum. *Surf. Sci.* **1987**, *185* (3), 495−514.

(7) Machan, C. W.; Kubiak, C. P. Electrocatalytic Reduction of Carbon Dioxide with Mn(terpyridine) Carbonyl Complexes. *Dalton Trans.* **2016**, *45* (43), 17179−17186.

(8) Knurr, B. J.; Weber, J. M. Solvent-Driven Reductive Activation of Carbon Dioxide by Gold Anions. *J. Am. Chem. Soc.* **2012**, *134* (45), 18804−18808.

(9) Gregoire, G.; Velasquez, J.; Duncan, M. A. Infrared Photodissociation Spectroscopy of Small Fe^+-$(CO_2)_n$ and Fe^+-$(CO_2)_n$ Ar Clusters. *Chem. Phys. Lett.* **2001**, *349* (5−6), 451−457.

(10) Tjelta, B. L.; Walter, D.; Armentrout, P. B. Determination of Weak Fe^+−L Bond Energies (L = Ar, Kr, Xe, N_2, and CO_2) by Ligand Exchange Reactions and Collision-Induced Dissociation. *Int. J. Mass Spectrom.* **2001**, *204* (1−3), 7−21.

(11) Armentrout, P. B.; Koizumi, H.; MacKenna, M. Sequential Bond Energies of $Fe^+(CO_2)_n$, n = 1−5, Determined by Threshold Collision-Induced Dissociation and ab Initio Theory. *J. Phys. Chem. A* **2005**, *109* (50), 11365−11375.

(12) Andersen, A.; Muntean, F.; Walter, D.; Rue, C.; Armentrout, P. B. Collision-Induced Dissociation and Theoretical Studies of Mg^+ complexes with CO, CO_2, NH_3, CH_4, CH_3OH, and C_6H_6. *J. Phys. Chem. A* **2000**, *104* (4), 692−705.

(13) Schwarz, H. Metal-Mediated Activation of Carbon Dioxide in the Gas Phase: Mechanistic Insight Derived from a Combined Experimental/Computational Approach. *Coord. Chem. Rev.* **2017**, *334*, 112−123.

(14) Dieterle, M.; Harvey, J. N.; Heinemann, C.; Schwarz, J.; Schroder, D.; Schwarz, H. Equilibrium Studies of Weakly Bound $Fe(L)^+$ Complexes with L = Xe, CO_2, N_2 and CH_4. *Chem. Phys. Lett.* **1997**, *277* (5−6), 399−405.

(15) Gregoire, G.; Brinkmann, N. R.; van Heijnsbergen, D.; Schaefer, H. F.; Duncan, M. A. Infrared Photodissociation Spectroscopy of $Mg^+(CO_2)_n$ and $Mg^+(CO_2)_n$ Ar Clusters. *J. Phys. Chem. A* **2003**, *107* (2), 218−227.

(16) Walters, R. S.; Brinkmann, N. R.; Schaefer, H. F.; Duncan, M. A. Infrared Photodissociation Spectroscopy of Mass-Selected $Al^+(CO_2)_n$ and $Al^+(CO_2)_n$ Ar Clusters. *J. Phys. Chem. A* **2003**, *107* (38), 7396−7405.

(17) Walker, N. R.; Grieves, G. A.; Walters, R. S.; Duncan, M. A. The Metal Coordination in $Ni^+(CO_2)_n$ and $NiO_2^+(CO_2)_m$ Complexes. *Chem. Phys. Lett.* **2003**, *380* (1−2), 230−236.

(18) Scurlock, C. T.; Pullins, S. H.; Duncan, M. A. Photodissociation Spectroscopy of Ca^+-CO_2. *J. Chem. Phys.* **1996**, *105* (9), 3579−3585.

(19) Iskra, A.; Gentleman, A. S.; Kartouzian, A.; Kent, M. J.; Sharp, A. P.; Mackenzie, S. R. Infrared Spectroscopy of Gas-Phase $M^+(CO_2)_n$ (M = Co, Rh, Ir) Ion−Molecule Complexes. *J. Phys. Chem. A* **2017**, *121* (1), 133−140.

(20) Ricks, A. M.; Brathwaite, A. D.; Duncan, M. A. IR Spectroscopy of Gas Phase $V(CO_2)_n^+$ Clusters: Solvation-Induced Electron Transfer and Activation of CO_2. *J. Phys. Chem. A* **2013**, *117* (45), 11490−11498.

(21) Griffin, J. B.; Armentrout, P. B. Guided Ion-Beam Studies of the Reactions of Fe_n^+ (n = 1−18) with CO_2: Iron Cluster Oxide Bond Energies. *J. Chem. Phys.* **1997**, *107* (14), 5345−5355.

(22) Knurr, B. J.; Weber, J. M. Solvent-Mediated Reduction of Carbon Dioxide in Anionic Complexes with Silver Atoms. *J. Phys. Chem. A* **2013**, *117* (41), 10764−10771.

(23) Knurr, B. J.; Weber, J. M. Structural Diversity of Copper-CO_2 Complexes: Infrared Spectra and Structures of $Cu(CO_2)_n^-$ Clusters. *J. Phys. Chem. A* **2014**, *118* (44), 10246−10251.

(24) Knurr, B. J.; Weber, J. M. Infrared Spectra and Structures of Anionic Complexes of Cobalt with Carbon Dioxide Ligands. *J. Phys. Chem. A* **2014**, *118* (23), 4056−4062.

(25) Knurr, B. J.; Weber, J. M. Interaction of Nickel with Carbon Dioxide in $[Ni(CO_2)_n]^-$ Clusters Studied by Infrared Spectroscopy. *J. Phys. Chem. A* **2014**, *118*, 8753−8757.

(26) Thompson, M. C.; Ramsay, J.; Weber, J. M. Solvent-Driven Reductive Activation of CO_2 by Bismuth: Switching from Metalloformate Complexes to Oxalate Products. *Angew. Chem., Int. Ed.* **2016**, *55* (48), 15171−15174.

(27) Thompson, M. C.; Dodson, L. G.; Weber, J. M. Structural Motifs of $[Fe(CO_2)_n]$- Clusters (n = 3 − 7). *J. Phys. Chem. A* **2017**, *121* (21), 4132−4138.

(28) Weber, J. M. A Pulsed Ion Source for the Preparation of Metal Containing Cluster Ions Using Supersonic Entrainment of Laser Vaporized Metal. *Rev. Sci. Instrum.* **2005**, *76*, 043301.

(29) Ahlrichs, R.; Bär, M.; Häser, M.; Horn, H.; Kölmel, C. Electronic-Structure Calculations on Workstation Computers - the Program System Turbomole. *Chem. Phys. Lett.* **1989**, *162* (3), 165−169.

(30) Lee, C. T.; Yang, W. T.; Parr, R. G. Development of the Colle-Salvetti Correlation-Energy Formula into a Functional of the Electron-

DOI: 10.1021/acs.jpca.7b06870
J. Phys. Chem. A 2017, 121, 7534−7542

Density. *Phys. Rev. B: Condens. Matter Mater. Phys.* **1988**, *37* (2), 785−789.
(31) Becke, A. D. Density-Functional Exchange-Energy Approximation with Correct Asymptotic-Behavior. *Phys. Rev. A: At., Mol., Opt. Phys.* **1988**, *38* (6), 3098−3100.
(32) Grimme, S. Semiempirical GGA-type Density Functional Constructed with a Long-Range Dispersion Correction. *J. Comput. Chem.* **2006**, *27* (15), 1787−1799.
(33) Weigend, F.; Ahlrichs, R. Balanced Basis Sets of Split Valence, Triple Zeta Valence and Quadruple Zeta Valence Quality for H to Rn: Design and Assessment of Accuracy. *Phys. Chem. Chem. Phys.* **2005**, *7* (18), 3297−3305.
(34) Deglmann, P.; Furche, F. Efficient Characterization of Stationary Points on Potential Energy Surfaces. *J. Chem. Phys.* **2002**, *117* (21), 9535−9538.
(35) Boese, A. D.; Schneider, H.; Gloess, A. N.; Weber, J. M. The Infrared Spectrum of $Au^{-}\cdot CO_2$. *J. Chem. Phys.* **2005**, *122*, 154301.
(36) Reed, A. E.; Weinstock, R. B.; Weinhold, F. Natural Population Analysis. *J. Chem. Phys.* **1985**, *83* (2), 735−746.
(37) Herzberg, G. *Molecular Spectra and Molecular Structure*; Krieger Publishing Co.: Malabar, FL, 1991; Vol. *III*.
(38) Shin, J. W.; Hammer, N. I.; Johnson, M. A.; Schneider, H.; Glöss, A.; Weber, J. M. An Infrared Investigation of the $(CO_2)_n^{-}$ Clusters: Core Ion Switching from both the Ion and Solvent Perspectives. *J. Phys. Chem. A* **2005**, *109* (14), 3146−3152.
(39) Walsh, A. D. 467. The Electronic Orbitals, Shapes, and Spectra of Polyatomic Molecules. Part II. Non-Hydride AB_2 and BAC Molecules. *J. Chem. Soc.* **1953**, *0*, 2266−2288.
(40) Myshakin, E. M.; Jordan, K. D.; Sibert, E. L.; Johnson, M. A. Large Anharmonic Effects in the Infrared Spectra of the Symmetrical $CH_3NO_2^{-}\cdot(H_2O)$ and $CH_3CO_2^{-}\cdot(H_2O)$ complexes. *J. Chem. Phys.* **2003**, *119* (19), 10138−10145.
(41) Schneider, H.; Boese, A. D.; Weber, J. M. Unusual Hydrogen Bonding Behavior in Binary Complexes of Coinage Metal Anions With Water. *J. Chem. Phys.* **2005**, *123*, 084307.
(42) Marcum, J. C.; Weber, J. M. Microhydration of Nitromethane Anions from Both a Solute and Solvent Perspective. *J. Phys. Chem. A* **2010**, *114* (34), 8933−8938.
(43) Dewar, M. J. S.; Zheng, Y.-J. Structure of the Oxalate Ion. *J. Mol. Struct.: THEOCHEM* **1990**, *209* (1), 157−162.
(44) Weber, J. M.; Schneider, H. Infrared Spectra of $X^{-}\cdot CO_2\cdot$Ar Cluster Anions (X= Cl,Br,I). *J. Chem. Phys.* **2004**, *120*, 10056.
(45) Walker, N. R.; Walters, R. S.; Duncan, M. A. Infrared Photodissociation Spectroscopy of $V^{+}(CO_2)_n$ and $V^{+}(CO_2)_n$Ar Complexes. *J. Chem. Phys.* **2004**, *120* (21), 10037−10045.
(46) Walker, N. R.; Walters, R. S.; Grieves, G. A.; Duncan, M. A. Growth Dynamics and Intracluster Reactions in $Ni^{+}(CO_2)_n$ Complexes via Infrared Spectroscopy. *J. Chem. Phys.* **2004**, *121* (21), 10498−10507.

DOI: 10.1021/acs.jpca.7b06870
J. Phys. Chem. A 2017, 121, 7534−7542